NEW-TPI Thermoplastic Polyimide: Structure and Relaxation Using SAXS and TSDC

SHARON XIN LU,[1] PEGGY CEBE,[1,*] and MALCOLM CAPEL[2]

[1]Department of Materials Science and Engineering, Massachusetts Institute of Technology, Cambridge, Massachusetts 02139; [2]Biology Department, Brookhaven National Synchrotron Light Source, Upton, New York 11973

SYNOPSIS

The thermoplastic polyimide Regulus™ NEW-TPI has been studied using small-angle X-ray scattering (SAXS) and thermally stimulated depolarization current (TSDC). SAXS was used to study the development of lamellar structure during isothermal or nonisothermal crystallization. The one-dimensional electron-density correlation function was used to determine structural parameters. The long period, lamellar thickness, and amorphous layer thickness increase as crystallization temperature increases from 300 to 360°C. By combining melting-point data with SAXS results, we report the side and fold surface free energies of NEW-TPI crystals, which are 29 ± 3 and 41 ± 3 erg/cm^2, respectively. Real-time SAXS was carried during nonisothermal cold-crystallization at 5°C/min. The long period decreases, while lamellar thickness, linear crystallinity, and interphase thickness increase, with increasing temperature. These changes are explained by a crystal-insertion model. TSDC was used as a more sensitive probe of the amorphous phase structure below 300°C. Both semicrystalline and amorphous NEW-TPI exhibit complex TSDC behavior. Above the glass transition, amorphous NEW-TPI has a strong TSDC peak attributed to short-range-ordered structures, which may serve as nucleation sites for subsequent crystallization. This peak was not seen in semicrystalline material. At the glass transition, both amorphous and semicrystalline NEW-TPI have a strong TSDC peak. In the semicrystalline polymer, relaxation of the amorphous dipoles is slightly restricted by the crystals, which results in a smaller relaxation peak and a shift to higher temperature. Below T_g, another TSDC peak occurs which is not due to dipolar relaxation. This peak is attributed to the combined effects of space charge, electrode type, ionizable species, and interfacial charges. © 1995 John Wiley & Sons, Inc.

INTRODUCTION

Aromatic polyimides have a unique structure and broad engineering applications. The imide and aromatic moieties in the monomer unit impart rigidity to the polymer chain, resulting in high thermal transition temperatures. Polyimides exhibit outstanding thermal stability and excellent mechanical properties, especially toughness. These materials also generally have low dielectric constant and dielectric loss, resulting in applications in electronic packaging and cable and wire insulation.

NEW-TPI, one of the important new members of the aromatic polyimide family, has been the recent subject of many research groups.[1-18] This novel polymer, a product of Mitsui Toatsu Chemical Co., is also a semicrystalline melt-processible material. Its monomer unit contains flexible ether and *meta*-phenyl linkages which lower its glass transition temperature (T_g) to 250°C.[1] The crystalline material has a melting temperature (T_m) of 385°C (DSC),[1,3] which enables NEW-TPI to be processed by standard thermoforming methods. Crystallinity is also likely to result in property enhancement, such as improving solvent resistance. According to our previous studies, NEW-TPI has a dielectric constant at 1 kHz of 3.2 and modulus of elasticity at room temperature of 3–4

* To whom correspondence should be addressed.

Journal of Applied Polymer Science, Vol. 57, 1359–1372 (1995)
 CCC 0021-8995/95/111359-14

GPa.[5,7] The chemical structure of NEW-TPI is shown below[1]:

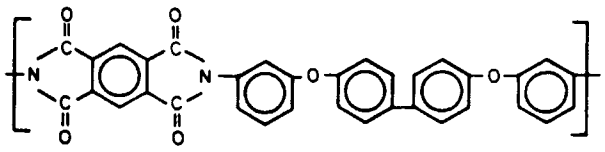

Characterization of the structure and properties of NEW-TPI has been reported by our group and others. Using X-ray diffraction, the NEW-TPI crystal structure was studied by Okuyama, et al.[2] Its thermal and rheological properties were studied by Hou and Reddy.[3] Brillhart and Cebe[9] determined the crystal lattice thermal expansion coefficient, while Lu et al.[10] reported lamellar stack and bulk thermal expansion properties. Morphology of spherulites was studied by Takahashi et al.[13] using transmission electron microscopy and by Hsiao et al.[11] using optical microscopy. Friler and Cebe[6] described the nonisothermal crystallization kinetics, while Huo et al.[4,5] first studied the isothermal cold-crystallization kinetics. We showed[5] that NEW-TPI crystallizes relatively slowly from the rubbery amorphous state. At a given crystallization temperature, the kinetics can be described by a single Avrami parameter over the entire crystallization process. As a function of crystallization temperature, a regime transition, from Regime II to Regime III, was observed in the growth kinetics at a temperature near 327°C, which was the temperature at which the fastest cold-crystallization occurred.[5]

These results were later confirmed by Hsiao et al.,[11] who reported on the isothermal melt-crystallization kinetics. These workers also determined spherulite growth rates and spherulite birefringence and suggested that radial growth occurs along the crystallographic b-axis. In the melt-crystallization study of Hsiao et al.,[11] discontinuities were observed in some of the parameters determined from small-angle X-ray scattering (SAXS) as a function of the melt-crystallization temperature, T_c. The long period, L, and lamellar thickness, l_c, both exhibited a jump, showing lower (and approximately constant) values for $T_c \leq 330$°C and higher values for $T_c \geq 340$°C. The temperature at which the break occurs is very close to the crystallization temperature at which fastest crystal growth occurs both for melt-[11] and for cold-crystallization.[5]

In this report, we continue our investigation of NEW-TPI using real-time SAXS to study the structure and thermally stimulated depolarization current (TSDC) to study relaxation behavior. SAXS is used to study the structure of NEW-TPI crystallized either isothermally or nonisothermally from the rubbery amorphous state. The long period, lamellar thickness, and crystallinity are obtained using the one-dimensional electron-density correlation function for NEW-TPI samples cold-crystallized at different temperatures. The relaxation behavior of NEW-TPI from −80 to 280°C was studied using TSDC. No sub-T_g relaxation is found within this temperature range, which may explain the relatively brittle mechanical behavior of the semicrystalline NEW-TPI.

EXPERIMENTAL

Characterization Techniques

A differential scanning calorimeter (DSC, Perkin-Elmer DSC-4) was used to study the crystallization and melting behavior of Regulus™ NEW-TPI. Indium was used to calibrate temperature and heat flow throughout our DSC study. The sample weight was around 8 mg and a scan rate of 10°C/min was used. Crystallinity was calculated from the endotherm area using the manufacturer's published value of 139 J/g as the heat of fusion of perfect crystalline NEW-TPI.[12]

WAXS experiments were carried out at room temperature in the reflection mode using a Rigaku RU-300 X-ray diffractometer with a diffracted beam graphite monochromator. The normal operating condition was 50 keV and 200 mA with CuKα radiation ($\lambda = 1.54$ Å). The scattering angle 2θ ranged from 5° to 55° with a step scan interval of 0.02° and a scan rate of 1°/min. Silicon powder (from National Institute of Standards and Technology) was rubbed on the sample surface to serve as a calibration standard for the peak position.

SAXS experiments were done at the Brookhaven National Synchrotron Light Source using a high-intensity X-radiation source in the transmission mode. The wavelength was 1.54 Å and the sample-to-detector distance was about 1.80 m calibrated using cholesteral meristate. The beam profile at the detector is 300 × 300 μm and, therefore, can be treated according to a pinhole geometry. The isotropic SAXS intensity was circularly integrated and normalized for changes in incident beam intensity and sample absorption. The background and thermal density fluctuations were subtracted from the normalized Lorentz-corrected scattered intensity. The one-dimensional electron-density correlation function was then calculated to obtain the long pe-

riod, lamellar thickness, and linear crystallinity of NEW-TPI, according to the method of Strobl and Schneider[19] for flat, parallel lamellae.

TSDC measurements were carried out on our self-designed and self-assembled apparatus. The major part is the sample cell which contains two layers. The first layer is for liquid nitrogen cooling. The second layer is for heating and Faraday shielding. The triaxially shielded electrical conduction path is concentric with the two layers of the cell. A polymer film sample is placed between a spring loaded pair of disc-shaped electrodes. Helium gas is used as a heat-transfer agent inside the cell, but the experiments were then conducted at a base pressure of about 1 Torr. To obtain a global TSDC spectrum, Regulus was first heated to a temperature T_p where the poling field is applied ($E_p = 1 \times 10^6$ V/m). After holding at T_p for 10 min, the cell was quickly quenched with liquid nitrogen at a cooling rate of about -15°C/min to a temperature T_0, where the poling field was reduced to zero and the two high-voltage electrodes were short-circuited to ground voltage. The current vs. temperature was recorded continuously during heating at a rate of 2°C/min. Unless otherwise mentioned, gold was evaporated on the samples to avoid the spurious charges that might come from the poor contact between the sample and the electrodes. Details about TSDC techniques have been discussed in some excellent reviews.[20-23]

Sample Preparation

Regulus NEW-TPI film, 100 μm thick, was supplied by Mr. Yasunori Sugita of Mitsui Toatsu Chemical Co. Figure 1 shows DSC scans of NEW-TPI as-received (AR), curve 1, and crystalline, curve 2. No crystallinity was detected in the AR sample from thermal analysis, optical birefringence, or wide-angle X-ray scattering (WAXS). The film was dried in a vacuum oven at 100°C for 20 h prior to any further treatment and it will be referred to as the amorphous sample. Some of the amorphous samples were cold-crystallized from 300 to 360°C until the completion of crystallization, as determined from our prior experiment.[5] For our TSDC experiment, two kinds of samples were prepared. One set was annealed at 260°C for 1 h. After annealing, the samples were either cooled to room temperature by air-quenching or cooled slowly to room temperature at 2°C/min. Another set of samples was cold-crystallized at 300°C for 1 h and quenched quickly to room temperature.

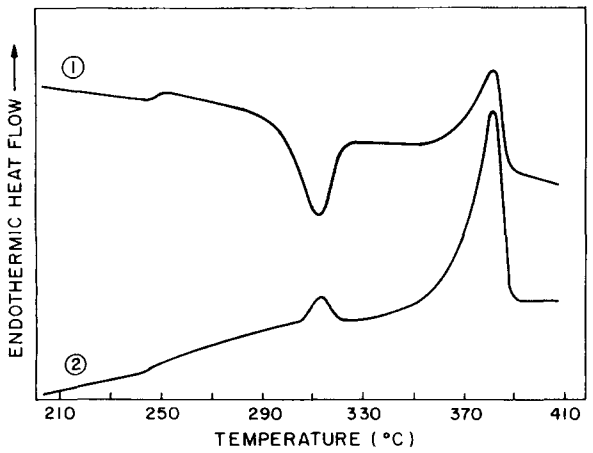

Figure 1 DSC scans at 10°C/min. for Regulus NEW-TPI amorphous film (curve 1) and semicrystalline film cold crystallized at 300°C for 1 h (curve 2).

RESULTS AND DISCUSSION

Room Temperature SAXS of Isothermally Cold-crystallized Samples

We show in Figure 2 the room-temperature, Lorentz-corrected SAXS intensity, Is^2, vs. the scattering vector, s ($s = 2 \sin \theta/\lambda$) for NEW-TPI samples cold-crystallized from 300 to 360°C. A systematic variation of peak position with cold-crystallization temperature T_c is observed. As T_c increases, the peak maximum shifts to smaller s. We assume that the structure consists of stacks of lamellae alternating with amorphous material. This assumption is justified since spherulites have been observed from Takahashi's TEM study of NEW-TPI.[13] A spherulitic structure and lamellar details have also been observed in other polyimides which were either crystallized from the melt and etched[24,25] or grown from solution.[26-28]

A discrete Fourier transform[29] was applied to the Lorentz-corrected intensity to obtain $K(z)$, the one-dimensional electron-density correlation function, as shown in the following equation:

$$K(z) = \sum_{j=1}^{N} 4\pi I_{\text{corr}} s^2 \omega_N^{(j-1)(z-1)} \tag{1}$$

where

$$\omega_N = e^{-2\pi i/N} \tag{2}$$

In eq. (1), z is the direction normal to lamellar stacks; N, the number of actual data points; and I_{corr}, the intensity corrected for background and thermal

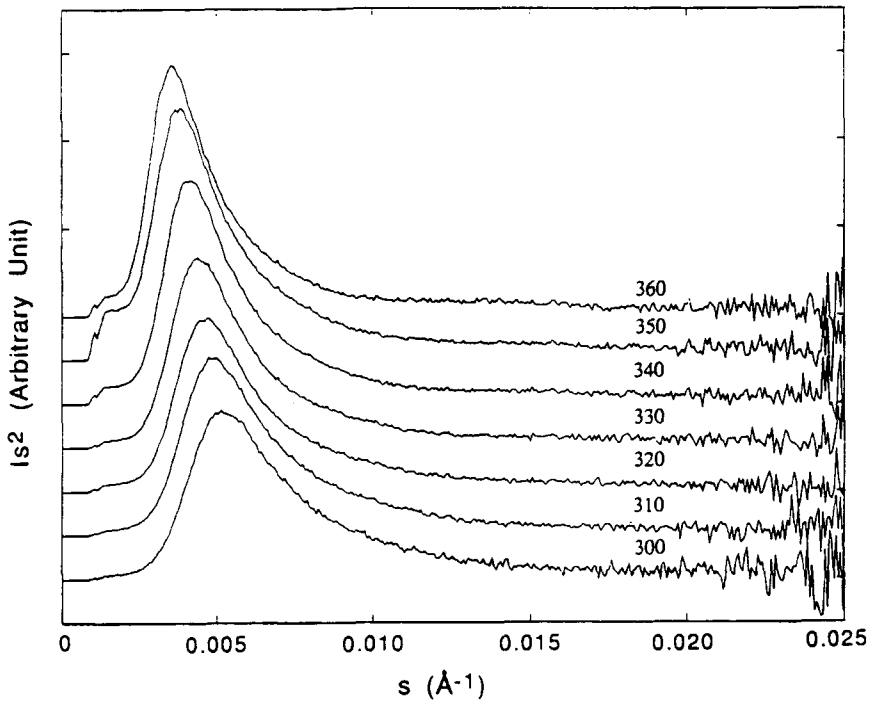

Figure 2 Lorentz-corrected SAXS intensity vs. scattering vector, s, for NEW-TPI cold-crystallized at the indicated temperatures (in °C).

density fluctuations. Linear extrapolation of intensity from the beam stop region to $s = 0$ was used in the summation. The resulting correlation function starts off with a z spacing of $1/s_{max}$, but a spline interpolation routine fills in the missing values in the region of interest. The treatment of Strobl and Schneider[19] was used for data analysis, but any effects of curvature of the lamellae were ignored.

From $K(z)$, we obtain the long period (squares) and lamellar thickness (triangles), and the results are plotted in Figure 3. Both the long period and lamellar crystal thickness show an increase with cold-crystallization temperature. The long period increases from 182 Å for $T_c = 300$°C to 264 Å for $T_c = 360$°C, while lamellar thickness increases from 52 to 76 Å over the same temperature range. [The low value of l_c at $T_c = 350$°C is attributed to measurement error. This error at $T_c = 350$°C appears in all quantities determined from $K(z)$]. Using a two-phase assumption, we write

$$L = l_c + l_a \tag{3}$$

where l_a is the amorphous layer thickness, also shown in Figure 3 (circles). Relatively more amorphous phase is included in between the lamellar stacks as cold-crystallization temperature increases. We see a change in the slope of L vs. T_c at 330°C. Below $T_c = 330$°C, L increases linearly with T_c. At 330°C, there is a slope change, and above $T_c = 330$°C, L once again increases linearly with T_c. We see no corresponding change in the lamellar thickness. Lamellar thickness generally changes linearly with T_c, increasing as the degree of undercooling (defined as $T_m^0 - T_c$) decreases. This, to-

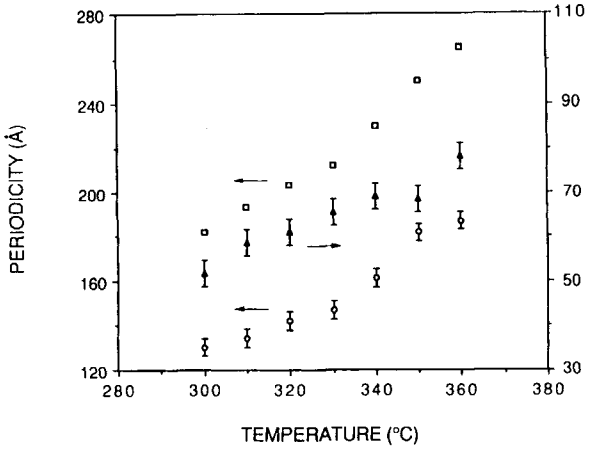

Figure 3 SAXS parameters as a function of cold-crystallization temperature for NEW-TPI: (□) long period and (○) amorphous layer thickness, both using left-hand vertical axis, and (▲) lamellar thickness, using right-hand vertical axis.

gether with the slope change in L vs. T_c, results in an increase in the amount of the amorphous phase that is contained between the lamellae ("interlamellar") at the higher crystallization temperatures (i.e., at lower degrees of undercooling). The increases in L and l_c with crystallization temperature have also been observed in other crystalline polymers and blends.[30-35]

We previously studied the cold-crystallization kinetics of NEW-TPI using isothermal DSC.[5] A slow crystallization rate is observed and the maximum crystallization rate occurs at around 327°C. We showed that the temperature at which the fastest cold-crystallization occurred served to divide the crystal growth into Regime II ($T_c \geq 327$°C) and Regime III ($T_c \leq 327$°C).[36] The temperature of the minimum was estimated from a single polynomial fit to the growth curve. Hsiao et al.[11] subsequently found the same regime transition in melt-crystallization studies, but the temperature at which the regime transition occurred was 340°C. Also, these workers reported a discontinuous change in both L and l_c for temperatures below or above the transition. The average long period changed from 170 Å ($T_c < 335$°C) to 194 Å ($T_c > 335$°C), while the average lamellar thickness changed from 120 to 135 Å.

In Figure 4, we present the crystallinity of NEW-TPI samples vs. cold-crystallization temperature. The linear crystallinity (circles) was obtained directly from the one-dimensional electron-density correlation function evaluated at room temperature. These values range from 0.33 to 0.30. (The extreme low value at $T_c = 350$°C is believed due to error in measurement.) The volume fraction crystallinity (squares) calculated from DSC data[5] ranges from 0.21 to 0.28. The volume fraction crystallinity, χ_c^v, was obtained from weight-average crystallinity, χ_c^w, using the following equation:

$$\chi_c^v = \frac{\chi_c^w(\rho_a/\rho_c)}{1 - \chi_c^w + \chi_c^w(\rho_a/\rho_c)} \tag{4}$$

where ρ_a and ρ_c are the amorphous phase and crystal phase densities, respectively. A linear relationship between density and volume fraction crystallinity has been assumed. We used $\rho_a = 1.33$ g/cm^3 (Ref. 12) and $\rho_c = 1.47$ g/cm^3 calculated from the unit cell structure.[2] In Figure 4, a slight decrease is observed for linear crystallinity obtained from the correlation function. However, within experimental error, the change can be considered minimal. At the same time, the volume fraction crystallinity calculated from DSC increases gradually. The difference between the two gets smaller as the cold-crystallization temperature increases.

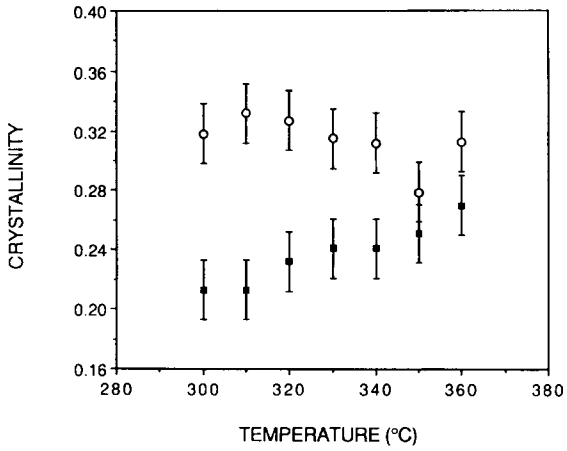

Figure 4 (○) Linear crystallinity from $K(z)$ and (■) volume crystallinity from DSC vs. cold-crystallization temperature for NEW-TPI.

The one-dimensional electron-density correlation function calculation is based on a model of very strict one-dimensional alternating lamellar stacks. The model assumes densely packed, isotropically distributed stacks of parallel lamellae. All stacks should obey the same internal statistics, and the system is a strict periodic two-phase system with low crystallinity. However, for cold-crystallized NEW-TPI, the arrangement of lamellar stacks may not follow the model's assumptions. For example, as we have discussed above, when the cold-crystallization temperature increases, more amorphous phase is included inside the lamellar stacks. However, any amorphous phase left outside the lamellar stacks during crystallization is undetectable. Therefore, the current calculation of linear crystallinity from $K(z)$ gives an overestimation of the crystalline-phase fraction compared to the crystallinity determined from DSC. The deviation becomes smaller as the cold-crystallization temperature increases, as seen in Figure 4, since more and more amorphous phase is included between the crystal lamellae.

Hsiao et al.[11] also determined the degree of crystallinity of NEW-TPI using both DSC and WAXS scattering. They assumed a linear relationship between mass fraction crystallinity (heat of fusion measurement) and density to determine a crystal heat of fusion of 116 J/g. However, when the mass fraction is used, the linear relationship is with the *specific volume* (inverse of density). This may be the reason that their heat of fusion value is considerably smaller than the value of 139 J/g suggested by Mitsui Toatsu.[12] These researchers also found that the

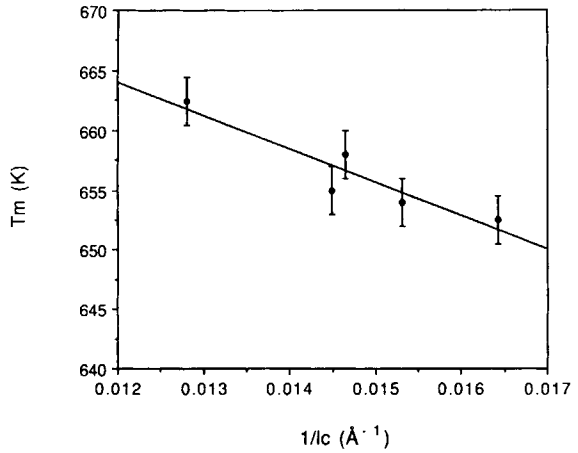

Figure 5 Melting temperature vs. 1/(lamellar thickness) for cold-crystallized NEW-TPI.

WAXS crystallinities ranged from 0.34 to 0.46 and linear crystallinities from $K(z)$ ranged from 0.71 to 0.67. The WAXS crystallinities were around 0.34–0.36 for $T_c < 350°C$, then jumped to 0.46 (350°C) and 0.42 (360°C). No trend with T_c was observed in linear crystallinity from $K(z)$.

The lamellar thickness derived from $K(z)$ is used to determine the thermodynamic melting temperature (T_m^0) and the polymer fold surface free energy (σ_e) using the following equation:[36]

$$T_m = T_m^0\left(1 - \frac{2\sigma_e}{\Delta H_f l_c}\right) \tag{5}$$

where T_m is the DSC melting temperature, and ΔH_f, the heat of fusion for 100% crystalline material. The results are shown in Figure 5. T_m^0 is found to be 424 ± 20°C, which is higher than previous published data of 400°C (Ref. 5) and 405°C.[11] The error bar on T_m^0 reflects the scatter in the data set. This scatter results in a correlation coefficient, $r^2 = 0.87$. Using T_m^0 of 424°C, ΔH_f of 139 J/g (Ref. 12) and crystal density of 1.47 g/cm^3,[2] we obtain the fold surface free energy, $\sigma_e = 41 \pm 3$ erg/cm^2. From spherulite growth-rate studies, Hsiao et al.[11] obtained the product, $\sigma\sigma_e$, which was 1176 erg^2/cm^4. This results in a side surface free energy, σ, of 29 ± 3 erg/cm^2. The close values of the side and fold surface free energies of NEW-TPI bear great similarity to another phenyl ring containing the polymer (PEEK) whose side and fold surface free energies were found to be 38 and 49 erg/cm^2, respectively.[37]

We expect in rigid chain polymers that the fold surface will be very irregular, consisting of very large folds. This would tend to reduce the work of chain folding and cause the fold surface and side surface free energies to be similar. Error bars on these surface free energies were determined by considering possible errors that may be introduced in our calculation of T_m^0 and σ_e. First, the lamellar thickness that we have obtained is the room temperature measurement. At the cold crystallization temperature, thermal expansion would give a slightly higher l_c. Second, it was found that crystal lamellae can thicken quite significantly at high temperature.[31] Compared to thermal expansion, this effect could be more pronounced. Nevertheless, using this l_c obtained from SAXS from Eq. (5) does allow us to calculate the side and fold surface free energies of NEW-TPI for the first time.

In a prior study of NEW-TPI,[5] the interphase thickness, d, was determined as a function of crystallization time at 300°C. Here, using the same formalism of Koberstein et al.,[38] we calculate interphase thickness as a function of cold-crystallization temperature, T_c, from

$$I_{\text{corr}}(s) = C\,e^{(-\pi^2 d^2 s^2)/s^4} \tag{6}$$

where C is a constant. Equation (6) holds only at large scattering vector. After transforming, we find that

$$\ln(I_{\text{corr}}(s)s^4) = \pi^2 d^2 s^2 + C \tag{7}$$

The interphase thickness is obtained at room temperature from the slope of $\ln(Is^4)$ vs. s^2 and is shown in Figure 6 as a function of the cold-crystallization temperature. A slight increase can be observed, although within experimental error, the change is small. The average interphase thickness is around

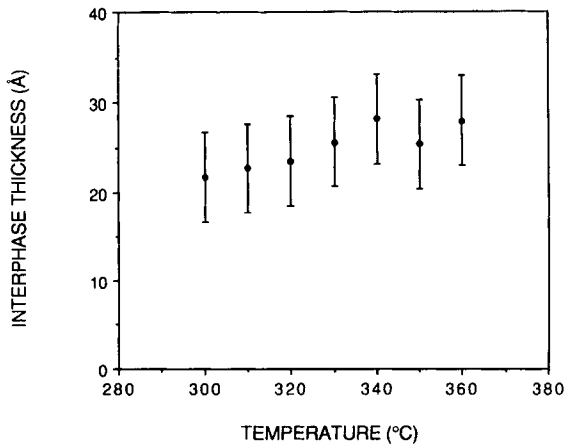

Figure 6 Interphase thickness of NEW-TPI as a function of cold-crystallization temperature.

23 Å, as compared to the monomer repeat unit, previously determined to be ~ 25 Å.[2,9] The interphase is the region over which the electron density decreases from that of the crystal to that of the isotropic amorphous phase. Whether or not this region corresponds to a fold surface is unknown in this polymer. Interphase thicknesses determined here as a function of crystallization temperature agree well with previous d values determined as a function of crystallization time.[5] The interphase thickness is smaller than the average value of lamellar thickness: l_c ranges from two to three times the monomer repeat unit length.

Real-time SAXS Study of Nonisothermal Cold-crystallization

We have carried a real-time SAXS experiment during nonisothermal cold-crystallization of NEW-TPI. The amorphous sample was heated from 250 to 350°C at a rate of 5°C/min and the data collection period was 30 s. The Lorentz-corrected SAXS intensity vs. s is shown in Figure 7. Two temperatures are marked in Figure 7, representing scans taken 1 min apart. No scattering peak develops until the temperature reaches 300°C. After that, a strong scattering peak starts to grow quite rapidly and shifts to a lower s, indicating the beginning of the crystallization and crystal growth. As the temperature increases, the peak becomes sharper and the intensity gets stronger. No significant shift in peak position is observed over the temperature range from 330 to 350°C.

The same data analysis method has been used as discussed in the previous section, and the results are shown in Figure 8. Figure 8(a) shows the long period as a function of measured temperature. Each data point represents an average over 2.5°. A significant drop in the long period starts around 305°C. L decreases from 245 Å and levels at about 203 Å when temperature reaches 322.5°C. This temperature is quite close to 327°C, the temperature at which NEW-TPI has its fastest crystallization rate.[5] The long period then increases only slightly until melting begins at a temperature of 350°C. In Figure 8(b), we present the lamellar thickness as a function of temperature. A lamellar thickness of 42 Å increases gradually to 60 Å, as temperature increases from 305 to 315°C, then levels off showing only a very slight decrease until the temperature reaches 350°C. In Figure 8(c), we present the linear fraction crystallinity as a function of measurement temperature. Crystallinity increases from 0.05 to 0.30 as temperature in-

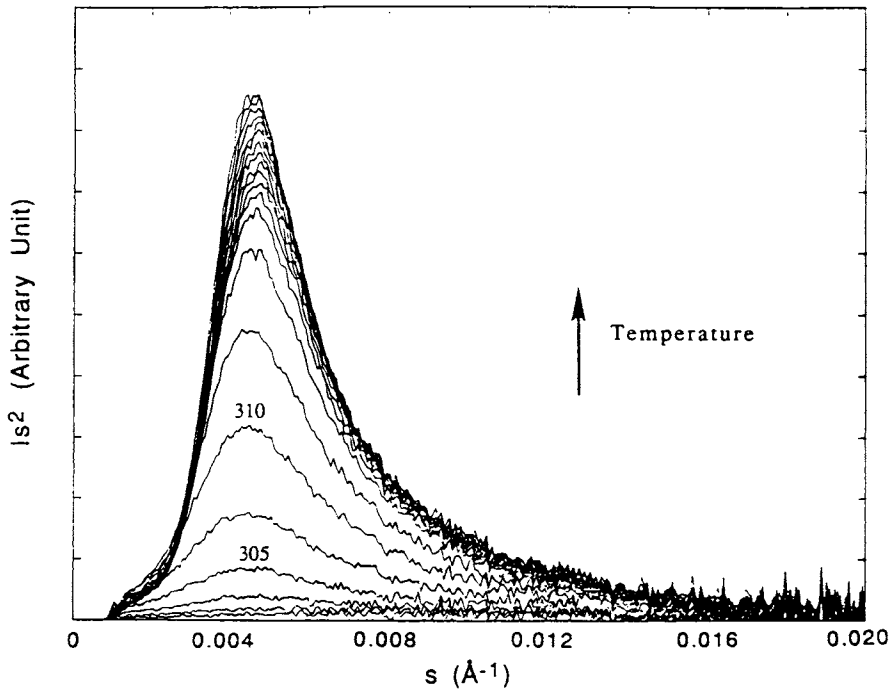

Figure 7 Lorentz-corrected SAXS intensity, Is^2, vs. scattering vector, s, during nonisothermal cold-crystallization of NEW-TPI at 5°C/min heating rate. Temperature is marked for two traces taken 1 min apart.

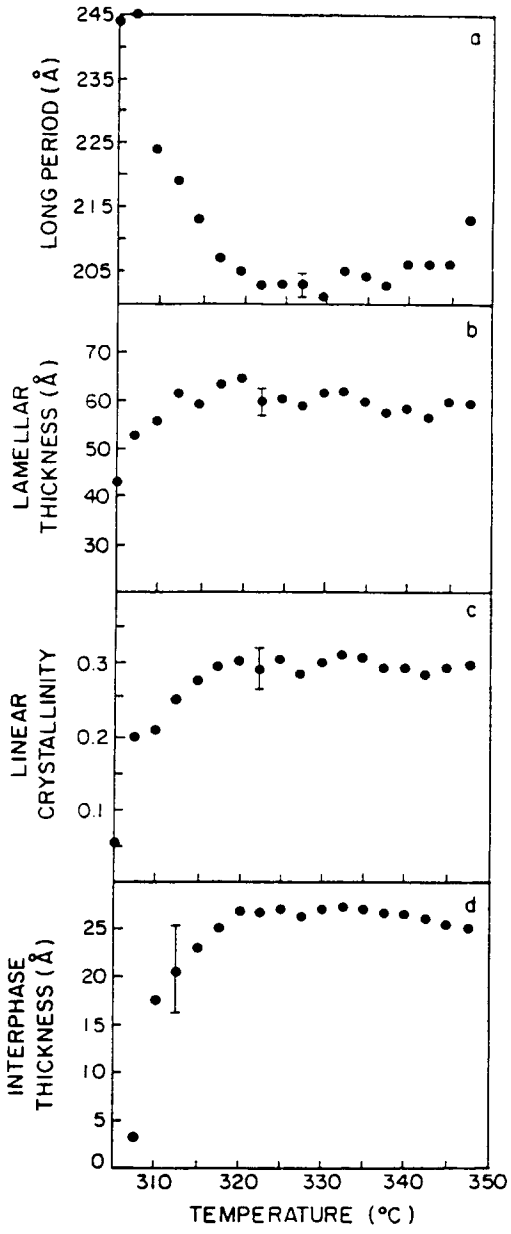

Figure 8 SAXS parameters as a function of temperature during nonisothermal crystallization of NEW-TPI at 5°C/min: (a) long period; (b) lamellar thickness; (c) linear crystallinity; (d) interphase thickness.

creases to 320°C and then remains constant until 350°C.

Similar changes in the long period and lamellar thickness were observed in our previous isothermal SAXS study,[5] indicating that the same crystallization mechanism is followed in both isothermal and nonisothermal crystallization. These observations could be explained by a lamellar insertion mechanism, which was first proposed by Keller[39] and later was used by Hsiao et al.[30,31] in their isothermal crystallization study of PEEK. In this model, it has been suggested that some thinner lamellae form between existing crystal lamellae as crystallization proceeds. This mechanism can explain why the average long period and the average lamellar thickness both decrease as crystallization time increases during isothermal crystallization.

This model may be used to explain our current data. At the beginning of the nonisothermal crystallization process, the crystals are very small and, therefore, the distance between lamellae is large. As the temperature increases, more and more lamellae are formed, causing a decrease in the average long period. At the same time, the already-formed crystals are also growing in thickness and newly formed lamellae are crystallizing at higher temperature. Both effects will tend to increase the average lamellar thickness. When the temperature approaches the temperature of the fastest crystallization (327°C), a relatively stable lamellar structure consisting of firmly packed alternating lamellar and amorphous phases is formed. Now we observe that L, l_c, and linear crystallinity all approach stable values. The crystal structure formed during nonisothermal crystallization is initially not well organized and can change to a more stable state with either crystallization time or temperature. In our case, as temperature increases, we observe a slight increase in L, caused by the removal of the thinner crystals.

We calculated the interphase thickness as a function of temperature using eqs. (6) and (7). The results are shown in Figure 8(d). Interphase thickness increases with temperature during nonisothermal crystallization and reaches a steady value of about 25 Å when temperature reaches 320°C. The temperature at which the interphase thickness becomes constant agrees well with previous changes seen in the lamellar thickness and crystallinity. This suggests that the interphase formation is related to crystal formation in such a way that they reach steady values at the same time, when the polymer structure is formed and relatively stabilized.

TSDC Study of NEW-TPI

SAXS is an excellent analytical method to study the development of the crystal structure of NEW-TPI after sufficient long-range order has been established to provide electron-density contrast. However, the method is difficult to apply prior to the appearance of periodic structure. Therefore, we adopted another analytical method, TSDC, to study the amorphous phase relaxation behavior for both amorphous and semicrystalline NEW-TPI. Relaxation of dipoles is

directly related to the microscopic environment (structure) in the amorphous phase. The temperatures chosen for TSDC studies are well below those at which crystalline dipoles are active.[6] TSDC results are shown in Figure 9 for amorphous NEW-TPI and in Figure 10 for semicrystalline NEW-TPI.

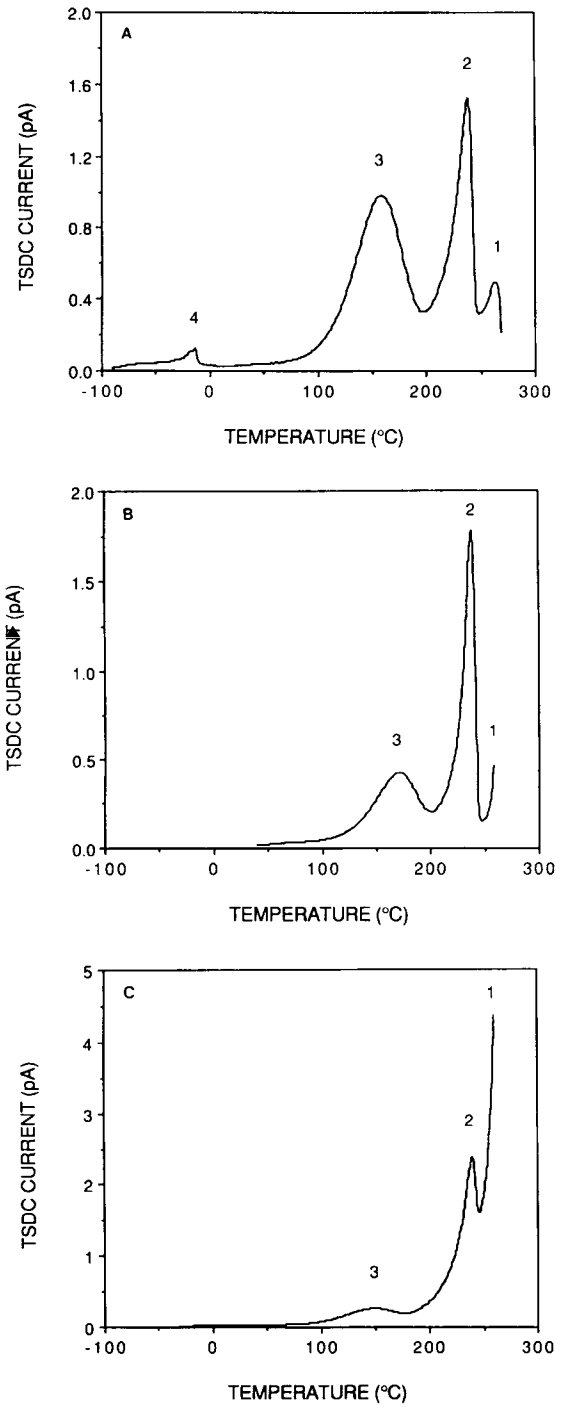

Figure 9 TSDC current vs. temperature for amorphous NEW-TPI poled at 250°C under different experimental conditions: (a) Au-coated, fast-quenched; (b) Au-coated, slow-cooled; (c) Al-coated, fast-quenched. Refer to text for description of numbered peaks.

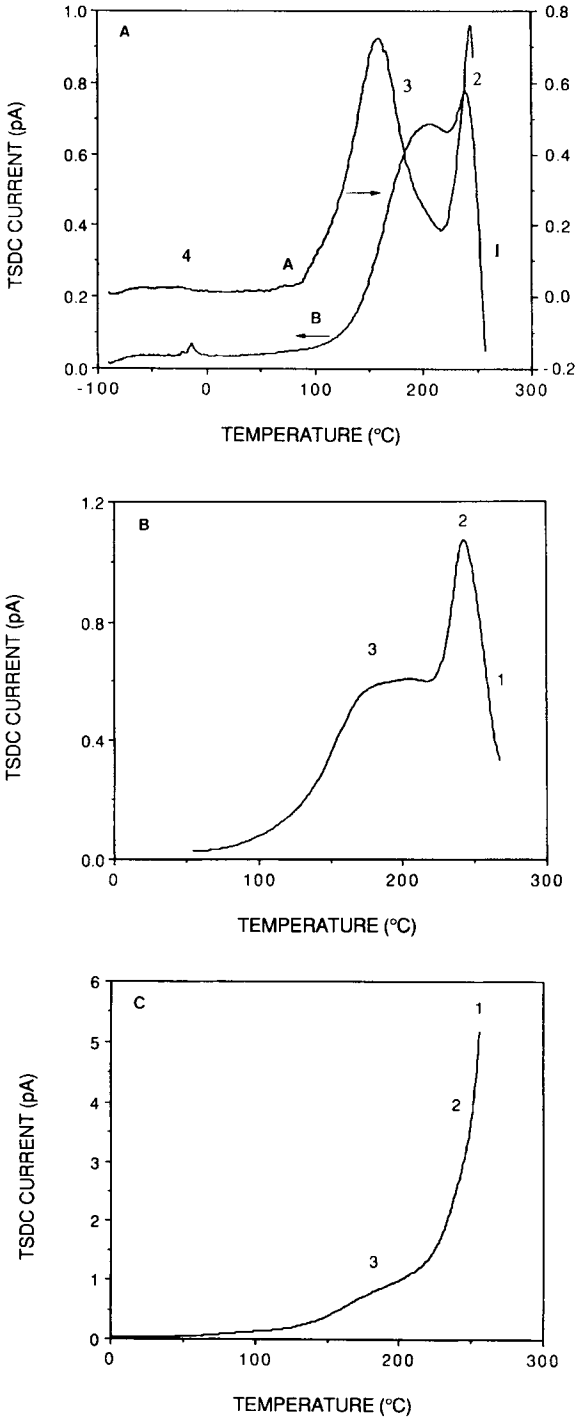

Figure 10 TSDC current vs. temperature for semicrystalline NEW-TPI poled at 250°C under different experimental conditions: (a) Au-coated, fast-quenched; (b) Au-coated, slow-cooled; (c) Al-coated, fast-quenched. Refer to text for description of numbered peaks.

TSDC Study of Amorphous NEW-TPI

We first performed a global TSDC study of amorphous NEW-TPI relaxed at 260°C for 1 h. The sample was coated with thermally evaporated Au and then poled at 250°C and fast-quenched. Results are shown in Figure 9(a) for temperatures ranging from −80 to 270°C. Four TSDC peaks are labeled from high to low temperature. A small peak, Peak 1, is observed at 265°C, which is above the glass transition temperature. Since no crystal peaks from Bragg scattering were seen[40,41] when WAXS was used to examine this sample after the TSDC tests, we conclude that the sample had not been crystallized.

However, we want to compare in Figure 11 the WAXS scans for this TSDC sample (curve 2) with a semicrystalline sample (curve 1) which had been cold-crystallized at 300°C for 1 h and with an amorphous film (curve 3) which had been relaxed at 260°C for 1 h. The shape of the TSDC amorphous halo was very similar to the shape underneath the semicrystalline sample and dissimilar to the halo of the relaxed amorphous sample. These results indicate a change in the state of the order of the amorphous phase when the TSDC sample is heated to 270°C. We conclude that Peak 1 is due to the formation of short-range order in the amorphous phase prior to crystallization of NEW-TPI. This observation agrees well with our previous dielectric experiment data where we observed a high-temperature shoulder just above T_g on the amorphous sample.[4] It is also consistent with our previous nonisothermal crystallization study[6] which showed that no crystals form below 270°C for the heating rate used here.

Three more peaks are observed in Figure 9(a). Peak 2 at 239°C has the largest current, with a peak height of 1.5 pA. Peak 3, observed at 159°C, is much broader and has a peak current around 1 pA. Peak 4, at −13°C, is quite small and sharp, covering only a 10° spread and was not reproducible. It shifted in position and sometimes disappeared entirely. This suggests that it must come from spurious charges, and we will not consider this peak further.

Peak 2 in Figure 9(a) comes from the glass transition relaxation of the sample. It occurs at the temperature at which long-range cooperative motion of the polymer chains becomes possible, and the dipoles, frozen by the poling/quenching process, are liberated. The glass transition temperature found from TSDC is about 10°C lower than that from DSC and the peak is spread over about 50°. Our observation is also in good agreement with Hsiao et al.

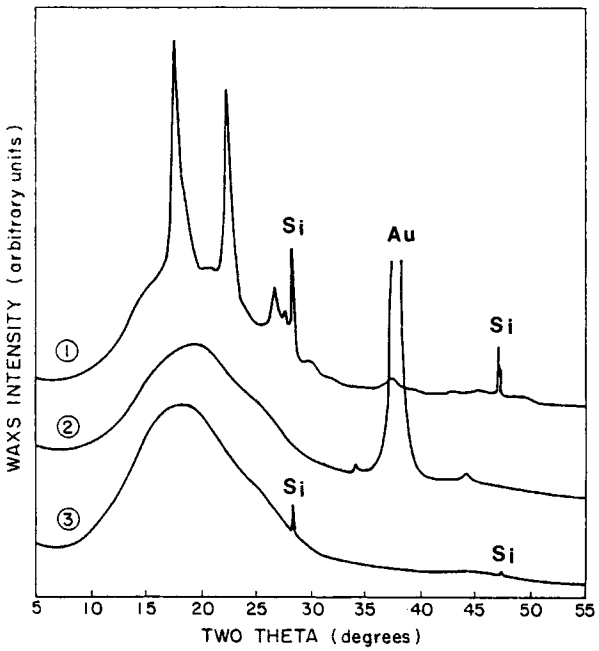

Figure 11 WAXS intensity vs. scattering angle, 2θ, for NEW-TPI semicrystalline film (curve 1) cold-crystallized at 300°C for 1 h, amorphous sample used in TSDC test heated to 270°C (curve 2), and amorphous sample (curve 3) relaxed at 260°C for 1 h. Silicon reference standard powder and gold coating on the TSDC sample contribute several peaks as marked.

who found T_g = 244°C at a heating rate of 7°C/min.[11] If we use van Turnhout's frequency equation[42,43] to obtain an equivalent TSDC frequency, the present data are consistent with the WLF plot from our previous dielectric and mechanical relaxation study.[4] The observation of a lower T_g under the comparatively lower frequency of the TSDC test is consistent with the manufacturer's quoted heat-distortion temperature, which is 238°C for amorphous NEW-TPI.[12]

Peak 3 is the peak with second highest current. The peak transition is not as sharp as Peak 2 and is spread out over about 100°C. Although our previous dielectric and mechanical relaxation measurements did not show any transition at this temperature range, Hsiao et al.[11] previously reported a TSDC peak in this temperature region attributed to electrode-surface effects. To establish whether this peak can be a dipole relaxation, we carried out a lower temperature 160°C poling TSDC experiment.[41] This poling temperature was chosen because it is the location of the current maximum of Peak 3. No depolarization current peak was observed in the temperature range from 0 to 180°C. This is

strong evidence that no dipolar relaxation is involved in Peak 3.[11,40,41]

A possible origin of this sub-T_g peak is considered to relate to space charge in the polymer. In most cases studied, space charge peaks, or ρ-peaks, occur above the glass transition temperature.[21] Free charge carriers may be created in the material at elevated temperature as a result of ionization of species left as residue of the initial processing and/or as a result of injection of carriers from the electrodes. Upon application of the electric field during poling, charge separation/injection may occur, and the charge mobility is reduced during the cooling stage. During the TSDC measurement, these charges become mobile as a function of increasing temperature and contribute to Peak 3. To verify the origin of Peak 3, we carried out two TSDC experiments and the results are shown in Figure 9(b) and (c) for comparison.

The first experiment that we did is the slow-cooling experiment. It is well known that the polymer free volume can be reduced by slow cooling through the glass transition region, as the amorphous phase approaches a more dense state. This treatment is similar to physical aging, in which the glassy polymer is held for a period of time at or below its glass transition temperature. Thus, a reduced free carrier mobility would be expected because of a reduction in free volume. In this experiment, a Au-coated amorphous sample was poled at 250°C and slowly cooled. The results are shown in Figure 9(b). Peak 1 was not observed because the test was stopped at too low a temperature. The glass transition, Peak 2, is at the same location and about the same peak current as those of the rapidly cooled sample of Figure 9(b). Slow cooling results in a more homogeneous distribution of dipoles and, consequently, a narrower Peak 2. Peak 3 is found to have a greatly reduced height, while its peak position shifts about 10°C to higher temperature. These changes agree with our previous expectation that reduced free volume leads to the impeded ability of the free carriers to move through the material.

The second TSDC experiment involves changing the electrode material to alter the work function of the electrodes relative to the polymer. Here, we used Al instead of Au as the electrode material. The sample was poled at 250°C and cooled rapidly followed by a subsequent heating. The TSDC results are shown in Figure 9(c). We see that Peak 1 (previously occurring at 265°C) is hidden under a steeply increasing current after T_g. Peak 2 at 239°C is also superimposed upon this current. This phenomenon is never observed on samples with gold electrodes, which suggests a different contacting mechanism for Au and Al with respect to NEW-TPI. The sharp current that we observed is therefore a result of contact charging that causes conduction in the polymer above T_g. Peak 3 is observed with a much smaller peak maximum and about 100°C spread. Compared to Peak 3 in Figure 9(a), its position shifts to a temperature 10°C lower and the relative ratio between Peaks 3 and 2 reduces from 0.64 (Au electrodes) to 0.22 (Al electrodes). This is additional strong evidence that Peak 3 originates from space-charge effects.

There are two possible reasons why there is no space-charge peak observed in the TSDC experiment where the sample is poled at 160°C.[41] First, although contact charging does exist at all temperatures, charge mobility through the sample depends not only on temperature but also on the physical state of the polymer. At 160°C, NEW-TPI is still in its glassy state; thus, the penetration of the charges created at the electrode–polymer surface is inhibited. Second, the ionizable species inside the polymer cannot move appreciably if the material is still in its glassy state. Therefore, no significant space-charge peak is observed when NEW-TPI was poled at 160°C.

To summarize the results from Figure 9(b) and (c), we conclude that Peak 3 observed in TSDC scans does not relate to secondary dipole relaxation. No sub-T_g relaxation is found in NEW-TPI for the temperature range of our study. This is not surprising if we consider its molecular structure. There are no side groups in the rigid monomer unit to give secondary relaxation. From the mechanical property point of view, the rigid main chain and no secondary relaxation would give NEW-TPI fewer energy-absorbing mechanisms during deformations.

TSDC Study of Semicrystalline NEW-TPI

Semicrystalline NEW-TPI films were cold-crystallized at 300°C for 1 h prior to gold coating. We adopted the same experimental conditions and same method of peak assignment for semicrystalline samples as for the amorphous sample described in the previous subsection. The resulting two global TSDC spectra are shown in Figure 10(a), samples A and B, for two independent trials of similarly treated films. Fresh samples were used in each case and the sample treatment and experimental conditions were identical. No peak is observed in region 1 in sample B (testing for sample A was halted at too low a temperature due to experimental difficulties). Since the crystal structure has already formed

in the semicrystalline samples, the amorphous phase is locked either in between the lamellar stacks or within the lamellar bundles. The amorphous phase mobility is constrained by the crystals. No additional short-range order can form when the temperature is below the treatment temperature. Therefore, no peak is observed for the semicrystalline samples in the temperature region where Peak 1 was seen in the amorphous sample. This observation provides additional confirmation of our previous assignment of Peak 1 in the amorphous polymer as due to the formation of short-range order prior to the crystallization. The glass transition, Peak 2, is seen in both samples at the same location and will be discussed in the following paragraph. Peak 3 appears in both samples A and B; however, it shifts its position. While Peak 3 occurred in all the semicrystalline and amorphous samples that we tested, its peak height and location were widely variable. We have not yet determined which stage of our sample treatment affects its location. As in the amorphous sample, Peak 4 comes from spurious charges and will not be considered further.

After carefully examining the glass transition relaxation peak, Peak 2 in Figure 10(a), we report the following observations which are very consistent with previous results. First, T_g of the semicrystalline polymer occurs at 244°C, which is 5°C above that of the amorphous sample. The crystals act as thermoreversible crosslinks and constrain amorphous phase mobility. This leads to slightly higher T_g in semicrystalline films. Second, this peak has a greater full width at half maximum than does the amorphous NEW-TPI, indicating a broader distribution of relaxation times in semicrystalline film. Third, the height of Peak 2 is also reduced in semicrystalline film. The relative peak height ratio of semicrystalline Peak 2 to amorphous Peak 2 is calculated to be 0.65. This may be related to the relative quantity of amorphous phase dipoles in the semicrystalline sample compared to the amorphous sample. Using DSC, our previous calculation of amorphous moieties from the step height of the heat-capacity change at T_g gave an amorphous fraction of 0.63 by weight.[5]

The origin of Peak 3, which in the amorphous sample we attributed to space charge and/or ionizable species inside the polymer bulk, appears to be even more complex in the semicrystalline sample.[44,45] Peak 3 for the semicrystalline NEW-TPI sample A [Fig. 10(a)] has a maximum at 159°C while Peak 3 in sample B has a maximum at 207°C. Generally speaking, there exist at least two phases inside the semicrystalline polymer bulk, i.e., the amorphous phase and crystalline phase, which provide current pathways of different conductivities. For semicrystalline NEW-TPI, in addition to the crystal phase, both mobile and rigid amorphous phases are observed[4,5] and different conductivity between them can be safely assumed. When the electric field is applied, homocharges will build up at the phase boundaries due to the differences in conductivity in addition to space charges and/or ionizable species inside the semicrystalline bulk. These factors come into play to give Peak 3.

Experiments have been carried out on semicrystalline NEW-TPI to further investigate the space charge effect of Peak 3. Figure 10(b) shows the result of TSDC measurement on semicrystalline sample slowly cooled after being poled at 250°C for 10 min. Again, Peak 1 was not observed because the polymer has already crystallized completely. The glass transition, Peak 2, is at the same location and about the same peak current as those of the rapidly cooled sample of Figure 10(a). No significant narrowing is observed, which suggests that the amorphous phase is constrained in between the crystalline phase and does not relax as it does in the pure amorphous polymer. Peak 3 broadens significantly in the slowly cooled sample. This is probably due to the longer separating distance of the charges and the impeded ability of the free carriers to move through the crystalline and amorphous interphase region.

Figure 10(c) shows the TSDC result for semicrystalline sample coated with aluminum electrodes, poled at 250°C for 10 min and cooled rapidly. Similar to what we have observed for the amorphous sample, the sample coated with Al shows ionic conduction[42,43] at high temperature, which suggests a different contact mechanism for Au and Al. This strong current starts to occur just below T_g and masks Peak 2. Peak 3 can be observed around 163°C but it is difficult to determine the peak shape. Combining these observations, it is clear that Peak 3 is not due to dipolar relaxation. Its origin is quite complicated, and space charge, electrode type, ionizable species, and interfacial charges can all contribute to its shape and position.

CONCLUSIONS

Regulus NEW-TPI has been studied by SAXS and TSDC. Both static and real-time SAXS have been employed to study the cold-crystallization behavior of NEW-TPI and to obtain crystallization parameters from the one-dimensional electron-density correlation function. We observed that both the long

period and lamellar thickness increase significantly with the isothermal cold-crystallization temperature, but linear crystallinity changes very little. Samples crystallized at a higher temperature contain a larger fraction of the amorphous phase between the crystal lamellae because of slower crystallization kinetics. In nonisothermal crystallization of NEW-TPI, lamellar thickness, crystallinity, and interphase thickness all increase with crystallization temperature and reach steady values at the same time. The long period drops at the beginning of the crystallization, then levels off as the temperature passes the region of fastest crystal growth.

TSDC has been used to study the relaxation behavior of NEW-TPI. The glass transition temperature of the semicrystalline polymer is only slightly higher than that of the amorphous sample. Thus, the crystals appear to have only a minor effect on the relaxation-time distribution of the amorphous chains. These results are consistent with our prior studies using DSC and dynamic mechanical relaxation.[4] Space charge, electrode type, ionizable species, and interfacial charges may all affect the TSDC spectrum.

This research was supported by the Electric Power Research Institute, Contract RP: 8007-13. The authors thank Mr. Yasunori Sugita from Mitsui Toatsu for film samples of Regulus™ and for support. The authors thank Prof. Lacabanne for helpful discussions about the TSDC cell design.

REFERENCES

1. P. M. Hergenrother, *SPE Conference on High Temperature Polymers and Their Uses,* Case Western Reserve University, Oct. 2–4, 1989.
2. K. Okuyama, H. Sakaitani, and H. Arikawa, *Macromolecules,* **25,** 7261 (1992).
3. T. H. Hou and R. M. Reddy, *SAMPE Q.,* **22**(2), 38 (1991).
4. P. P. Huo and P. Cebe, *Polymer,* **34,** 696 (1993).
5. P. P. Huo, J. B. Friler, and P. Cebe, *Polymer,* **34,** 4387 (1993).
6. J. B. Friler and P. Cebe, *Polym. Eng. Sci.,* **33,** 587 (1993).
7. Y. Aihara and P. Cebe, *Polym. Eng. Sci.,* **34,** 1275 (1993).
8. P. P. Huo and P. Cebe, *Colloid Polym. Sci.,* **270,** 840 (1992).
9. M. Brillhart and P. Cebe, *J. Polym. Sci. Polym. Phys. Ed.,* **33,** 927 (1995).
10. S. X. Lu, P. Cebe, and M. Capel, to appear.
11. B. Hsiao, B. Sauer, and A. Biswas, *J. Polym. Sci. Polym. Phys. Ed.,* **32,** 737 (1993).
12. Technical Data Sheet A-00, Mitsui Toatsu Chem., Inc., Tokyo, Japan.
13. S. Yuasa, M. Truji, and T. Takahashi, *Polym. Prepr. Jpn.,* **40,** 491 (1991).
14. T. Hirade, Y. Hama, T. Sasuga, and T. Seguchi, *Polymer,* **32,** 2499 (1991).
15. T. Sasuga, *Polymer,* **32,** 1539 (1991).
16. B. B. Sauer and B. S. Hsiao, *Polymer,* **34,** 3315 (1993).
17. K. G. Blizard and R. R. Haghighat, *Polym. Eng. Sci.,* **33,** 799 (1993).
18. N. Miyazaki, T. Hamao, and T. Munakata, *J. Soc. Mater. Sci. Jpn.,* **43,** 457 (1994).
19. G. R. Strobl and M. J. Schneider, *J. Polym. Sci. Polym. Phys. Ed.,* **18,** 1343 (1980).
20. P. Hedvig, in *Dielectric Spectroscopy of Polymers,* A. Hilger, Ed., Wiley, New York, 1977.
21. P. Braunlich, *Thermally Stimulated Relaxation in Solids,* Springer-Verlag, Berlin, 1979.
22. J. P. Ibar, P. Denning, T. Thomas, A. Bernes, C. de Goys, J. R. Saffell, P. Jones, and C. Lacabanne, in *Polymer Character: Physical Properties, Spectroscopic, and Chromatographic Methods,* Advances in Chemistry Series 227, American Chemical Society, Washington, DC, 1990, p. 167.
23. A. Bernes, R. F. Boyer, D. Chatain, C. Lacabanne, and J. P. Ibar, in *Order in the Amorphous State of Polymers,* S. E. Keinath, Ed., Plenum Press, London, 1987.
24. J. Muellerleile and G. Wilkes, *Polym. Commun.,* **32**(6), 176 (1991).
25. J. Muellerleile, B. Risch, D. Rodrigues, and G. Wilkes. *Polymer,* **34**(4), 789 (1993).
26. S. Cheng, Z. Wu, M. Eashoo, S. Hsu, and F. Harris. *Polymer,* **32**(10), 1803 (1991).
27. S. Cheng, J. Park, C. Lee, and F. Harris. *ACS Polym. Prepr.,* **34,** 774 (1993).
28. S. Cheng, M. Mittleman, J. Janimak, D. Shen, T. Chalmers, H. Lien, C. Tso, P. Gabori, and F. Harris. *ACS Polym. Prepr.,* **33,** 449 (1992).
29. Matlab Reference Guide, The Math Works Inc., Natic, 1992.
30. B. S. Hsiao, K. H. Gardner, D. Q. Wu, and B. Chu, *Polymer,* **34,** 3986 (1993).
31. B. S. Hsiao, K. H. Gardner, D. Q. Wu, and B. Chu, *Polymer,* **34,** 3996 (1993).
32. C. Santa Cruz, N. Stribeck, and H. G. Zachmann, *Macromolecules,* **24,** 5980 (1991).
33. H. H. Song, R. S. Stein, D. Q. Wu, M. Ree, J. C. Phillips, A. LeGrand, and B. Chu, *Macromolecules,* **21,** 1180 (1988).
34. H. H. Song, D. Q. Wu, B. Chu, M. Satkowski, M. Ree, R. S. Stein, and J. C. Phillips, *Macromolecules,* **23,** 2380 (1990).
35. K. Tashiro, M. M. Satkowski, R. S. Stein, Y. Li, B. Chu, and S. L. Hsu, *Macromolecules,* **25,** 1809 (1992).
36. J. D. Hoffman, G. T. Davis, and I. Lauritzen, in *Treatise on Solid State Chemistry,* N. B. Hanney, Ed., Plenum Press, New York, 1976.

37. D. J. Blundell and B. N. Osborn, *Polymer,* **24,** 953 (1983).
38. J. Koberstein, B. Morra, and R. Stein, *J. Appl. Crystallogr.,* **13,** 34 (1980).
39. A. Keller, *IUPAC Int. Symp., Macromol. Proc.,* Florence, 1980, p. 135.
40. S. X. Lu, W. C. Russell, and P. Cebe, *Proc. Mat. Res. Soc.,* **321,** 197 (1994).
41. S. X. Lu and P. Cebe, *ACS Proc. Div. Polym. Mater. Sci. Eng.,* **70,** 443 (1994).
42. J. van Turnhout, *Polym. J.,* **2,** 173 (1971).
43. J. van Turnhout, *Thermally Stimulated Discharge of Polymer Electrets,* Elsevier, Amsterdam, 1975.
44. N. Kumar and S. Chand, *Phys. Lett. A,* **119,** 185 (1986).
45. B. B. Sauer, P. Avakian, H. W. Starkweather, and B. S. Hsiao, *Macromolecules,* **23,** 5119 (1990).

Received November 28, 1994
Accepted March 19, 1995